

Indian Ocean Variability in the GFDL Coupled Climate Model

QIAN SONG

Program in Atmospheric and Oceanic Sciences, Princeton University, Princeton, New Jersey

GABRIEL A. VECCHI* AND ANTHONY J. ROSATI

National Oceanic and Atmospheric Administration/Geophysical Fluid Dynamics Laboratory, Princeton, New Jersey

(Manuscript received 2 May 2005, in final form 4 October 2005)

ABSTRACT

The interannual variability of the Indian Ocean, with particular focus on the Indian Ocean dipole/zonal mode (IODZM), is investigated in a 250-yr simulation of the GFDL coupled global general circulation model (CGCM). The CGCM successfully reproduces many fundamental characteristics of the climate system of the Indian Ocean. The character of the IODZM is explored, as are relationships between positive IODZM and El Niño events, through a composite analysis. The IODZM events in the CGCM grow through feedbacks between heat-content anomalies and SST-related atmospheric anomalies, particularly in the eastern tropical Indian Ocean. The composite IODZM events that co-occur with El Niño have stronger anomalies and a sharper east–west SSTA contrast than those that occur without El Niño. IODZM events, whether or not they occur with El Niño, are preceded by distinctive Indo-Pacific warm pool anomaly patterns in boreal spring: in the central Indian Ocean easterly surface winds, and in the western equatorial Pacific an eastward shift of deep convection, westerly surface winds, and warm sea surface temperature. However, delayed onsets of the anomaly patterns (e.g., boreal summer) are often not followed by IODZM events. The same anomaly patterns often precede El Niño, suggesting that the warm pool conditions favorable for both IODZM and El Niño are similar. Given that IODZM events can occur without El Niño, it is proposed that the observed IODZM–El Niño relation arises because the IODZM and El Niño are both large-scale phenomena in which variations of the Indo-Pacific warm pool deep convection plays a central role. Yet each phenomenon has its own dynamics and life cycle, allowing each to develop without the other.

The CGCM integration also shows substantial decadal modulation of the occurrence of IODZM events, which is found to be not in phase with that of El Niño events. There is a weak, though significant, negative correlation between the two. Moreover, the statistical relationship between the IODZM and El Niño displays strong decadal variability.

1. Introduction

The Indian Ocean exhibits variability on a wide range of scales. A distinctive feature of the Indian Ocean is the seasonally reversing monsoon circulation, which is manifested in physical, biological, and biogeochemical properties of the system (see Schott and McCreary 2001 and references therein). In addition, the Indian Ocean also exhibits substantial interannual and

longer time-scale variability (e.g., Allan et al. 1995; Murtugudde and Busalacchi 1999; Behera et al. 2000). Of particular interest are Indian Ocean dipole/zonal mode (IODZM) events (e.g., Saji et al. 1999; Webster et al. 1999; Annamalai and Murtugudde 2004). Indian Ocean interannual variability is of interest, in part because of its potential impacts on tropical Pacific interannual variability (Gutzler and Harrison 1987; Annamalai et al. 2005), and on the monsoons over south Asia, East Africa, and Australia (Annamalai and Murtugudde 2004; Vecchi and Harrison 2004). Efforts are under way to design and deploy an integrated Indian Ocean observing system in order to better understand and predict Indian Ocean variability (Meyers et al. 2000; Masumoto et al. 2003, 2005; CLIVAR–GOOS Indian Ocean Panel et al. 2007).

In the Indian Ocean, unlike in the other tropical

* UCAR Visiting Scientist Program.

Corresponding author address: Dr. Qian Song, NOAA/Geophysical Fluid Dynamics Laboratory, P.O. Box 308, 201 Forrestal Rd., Princeton, NJ 08542.
E-mail: qian.song@noaa.gov

ocean basins, the equatorial thermocline is deep and there is no persistent equatorial upwelling. These two features suggest that the strong thermocline–sea surface temperature (SST) feedbacks fundamental to the El Niño–Southern Oscillation (ENSO; Bjerknes 1969) are not active in the Indian Ocean. Thus, many studies have focused on the interannual Indian Ocean variability resulting from external forcing, in particular that driven by ENSO (e.g., Nigam and Shen 1993; Tourre and White 1995; Klein et al. 1999; Venzke et al. 2000; Lau and Nath 2003). The ENSO-related SST anomalies (SSTAs) in the Indian Ocean are basin wide and peak about one to two seasons after the maximum of the SSTAs in the central/eastern tropical Pacific (e.g., Harrison and Larkin 1998). These basin-wide ENSO-driven Indian Ocean SSTAs can be partially attributed to anomalous air–sea enthalpy and radiative fluxes, remotely forced by ENSO through an “atmospheric bridge” (Klein et al. 1999).

However, the lack of equatorial upwelling does not preclude coupled dynamics arising from Bjerknes-type feedbacks in the Indian Ocean, as there is upwelling along the coast of Somalia (boreal summer), off of Java–Sumatra (May–November), and in the open ocean in the southwest tropical Indian Ocean (year round) (Schott et al. 2002). In particular, because the upwelling region off Java–Sumatra is within the Indo-Pacific warm pool, oceanic changes can induce substantial air–sea feedbacks through changes in atmospheric convection (e.g., Murtugudde and Busalacchi 1999; Saji et al. 1999; Webster et al. 1999). Anomalous surface cooling in the eastern tropical Indian Ocean (ETIO) is often accompanied by anomalous surface warming in the western tropical Indian Ocean (WTIO); the resultant east–west SSTA gradient has been employed to define the IODZM (e.g., Saji et al. 1999; Webster et al. 1999; Murtugudde et al. 2003), a name that is questioned by some studies (e.g., Hasternrath 2002).

The extent to which the IODZM is a free coupled mode or whether external triggers may be needed for its initiation remains a topic of active discussion (Annamalai et al. 2003; Gualdi et al. 2003; Li et al. 2003; Loschnigg et al. 2003; Lau and Nath 2004). In particular, the relationship between the IODZM and ENSO continues to be debated (e.g., Allan et al. 2001; Baquero-Bernal et al. 2002; Huang and Kinter 2002; Krishnamurthy and Kirtman 2003; Li et al. 2003). It has been argued that because IODZM events have occurred without El Niño (e.g., 1961, 1994) and there are only weak correlations between the IODZM index and ENSO indices, the IODZM is a mode independent of ENSO (e.g., Saji et al. 1999; Iizuka et al. 2000; Rao et al. 2002). However, it has been noted that, because sea-

sonally stratified correlations between the IODZM index and ENSO indices become substantially higher, aspects of the IODZM may be considered as forced by ENSO (e.g., Xie et al. 2002; Baquero-Bernal et al. 2002; Gualdi et al. 2003).

Much has been learned about the IODZM from observations (e.g., Webster et al. 1999; Rao et al. 2002; Xie et al. 2002; Annamalai et al. 2003; Saji and Yamagata 2003) or ocean-only models (e.g., Behera et al. 1999; Murtugudde et al. 2000; Li et al. 2002; Vinayachandran et al. 2002). However, to investigate the nature of the IODZM and to isolate internal Indian Ocean variability from that forced by ENSO, coupled general circulation models (CGCMs) are necessary. Despite several CGCM studies on the IODZM (e.g., Iizuka et al. 2000; Gualdi et al. 2003; Loschnigg et al. 2003; Lau and Nath 2004; Wajsovicz 2004), questions of fundamental importance still remain unresolved, such as the initiation processes for IODZM events, the relation between IODZM and ENSO, and the decadal variation of the IODZM.

Recently, a state-of-the-art CGCM has been developed at the U.S. National Oceanic and Atmospheric Administration’s Geophysical Fluid Dynamics Laboratory (NOAA/GFDL), and multicentury integrations with it provide a fresh opportunity to further explore the IODZM. In this study, we analyze a 250-yr simulation in the GFDL CM2.1 global coupled climate model to study the interannual variability of the Indian Ocean, with principal focus on the IODZM, and examine the pending questions about the IODZM mentioned earlier. This study also serves as an assessment and documentation of Indian Ocean variability in this GFDL CGCM, which is also being employed to conduct climate sensitivity experiments for the fourth assessment of the Intergovernmental Panel for Climate Change (IPCC).

This paper is organized as follows. Section 2 describes the GFDL coupled model. In section 3 we characterize the model simulation of the Indian Ocean seasonal climatology. We focus on the interannual Indian Ocean SST variability and the statistical characteristics of the IODZM simulated in the model in section 4. We perform a composite analysis of the IODZM and ENSO in section 5. In section 6 the decadal variations of the occurrence of IODZM events and the IODZM–ENSO relation are studied. In section 7 we discuss some of our findings, and our conclusions are presented in section 8.

2. Model description

The model used in this study is the GFDL CM2.1 ocean–atmosphere–land–ice global CGCM. Details of

the model formulation are documented in Gnanadesikan et al. (2006, ocean model), GFDL Global Atmospheric Model Development Team (2004, atmosphere and land model), Delworth et al. (2006, coupled model), Wittenberg et al. (2006, ENSO), and Stouffer et al. (2006, climate sensitivity). Here, only a brief description of the coupled model is provided.

The ocean component of the coupled model is based on the Modular Ocean Model version 4 code (Griffies et al. 2003), and has 50 vertical layers (with 10-m resolution in the upper 220 m). The horizontal resolution is $1^\circ \times 1^\circ$ and the meridional resolution reduces to $\frac{1}{3}^\circ$ equatorward of 15° . Diurnally varying insolation is used, and shortwave penetration depth is specified as spatially and climatologically varying. The model has an explicit free surface, with explicit freshwater fluxes between ocean, land, the cryosphere, and the atmosphere. The mixed layer is predicted using the K-profile parameterization (Large et al. 1994). The eddy mixing parameterization of Gent and McWilliams (1990) as implemented by Griffies (1998) is used in the model.

The atmosphere component is the GFDL atmosphere model AM2p12b (GFDL Global Atmospheric Model Development Team 2004). The model has a finite-volume dynamical core, with 24 vertical layers and $2.5^\circ \times 2^\circ$ horizontal spacing. A K-profile planetary boundary layer scheme, relaxed Arakawa–Schubert convection, and a parameterization of the vertical momentum transport by cumulus convection are employed in the model.

Different components of the GFDL CM2.1 model are coupled through the Flexible Modeling System (see online at <http://www.gfdl.noaa.gov/~fms/>). The atmosphere, ocean, land, and sea ice exchange fluxes every 2 h, and fluxes are conserved within machine precision. The particular coupled experiment we study is the so-called 1990 control run, where 1990 values of tracer gases, insolation, aerosols, and land cover are applied. This experiment is also a control experiment for the suite of experiments GFDL has conducted for the fourth assessment of the IPCC. The coupled model is run without flux adjustment for 300 yr and produces a realistic simulation of many aspects of the global climate (e.g., Delworth et al. 2006; Gnanadesikan et al. 2006; Wittenberg et al. 2006). To reduce the effects of the initial adjustment, we analyze the model simulation of years 51–300 in this study.

Detailed discussion of the model representation of ENSO can be found in Wittenberg et al. (2006). Briefly, the model has a robust ENSO with an irregular period between 2 and 5 yr, a distribution of SSTAs that is skewed toward warm events, a realistic evolution of subsurface temperature anomalies, realistic correla-

tions with precipitation anomalies outside the tropical Pacific, and substantial multidecadal fluctuation in amplitude. However, the simulated ENSO events are too strong, and the anomalous SST, wind stress, and precipitation patterns are shifted 20° – 30° west of observed.

3. Indian Ocean climatology

We here discuss the CGCM simulation of the Indian Ocean seasonal climatologies (calculated from model simulation of years 51–300) of SST, precipitation, thermocline depth, and surface winds (Figs. 1 and 2). We use as our observational comparisons the Levitus ocean temperature climatology (Levitus 1994), the European Centre for Medium-Range Weather Forecasts (ECMWF) surface winds (over the period of 1986–2001), the Climate Prediction Center's Merged Analysis of Precipitation dataset (Xie and Arkin 1996), and the Climate Prediction Center outgoing longwave radiation (OLR) data (over the period 1975–2004).¹

a. Surface winds

The model reproduces the monsoonal reversal of winds over the northern Indian Ocean: the southwestlies during boreal summer and the northeasterlies during boreal winter (Fig. 1). Since the magnitude of the surface winds during boreal summer is larger than that in other seasons, the annual mean wind field is dominated by the boreal summer wind pattern (not shown). The magnitude of the surface winds in the model is slightly (1 – 2 m s^{-1}) stronger than that of the winds from the ECMWF product, particularly in the Southern Hemisphere.

The climatological equatorial winds in both ECMWF and the CGCM reverse direction four times a year with westerlies during the monsoon transition seasons (peak in May and October) and easterlies during the monsoon seasons. The equatorial westerlies during the transition seasons—in both the model and observations—drive eastward-flowing Wyrtki (1973) jets (not shown). The modeled equatorial westerlies during the monsoon transition seasons are 1 – 2 m s^{-1} weaker than those in the ECMWF climatology; thus, the modeled Wyrtki jets are weaker than those estimated from ship drift and drifter data (Cutler and Swallow 1984; Richardson and McKee 1989) by $\sim 5 \text{ cm s}^{-1}$. The annual mean equatorial zonal wind in the model is westerly, which is a

¹ Precipitation and OLR data made available by NOAA's Climate Diagnostics Center (information available online at <http://cdc.noaa.gov/>).

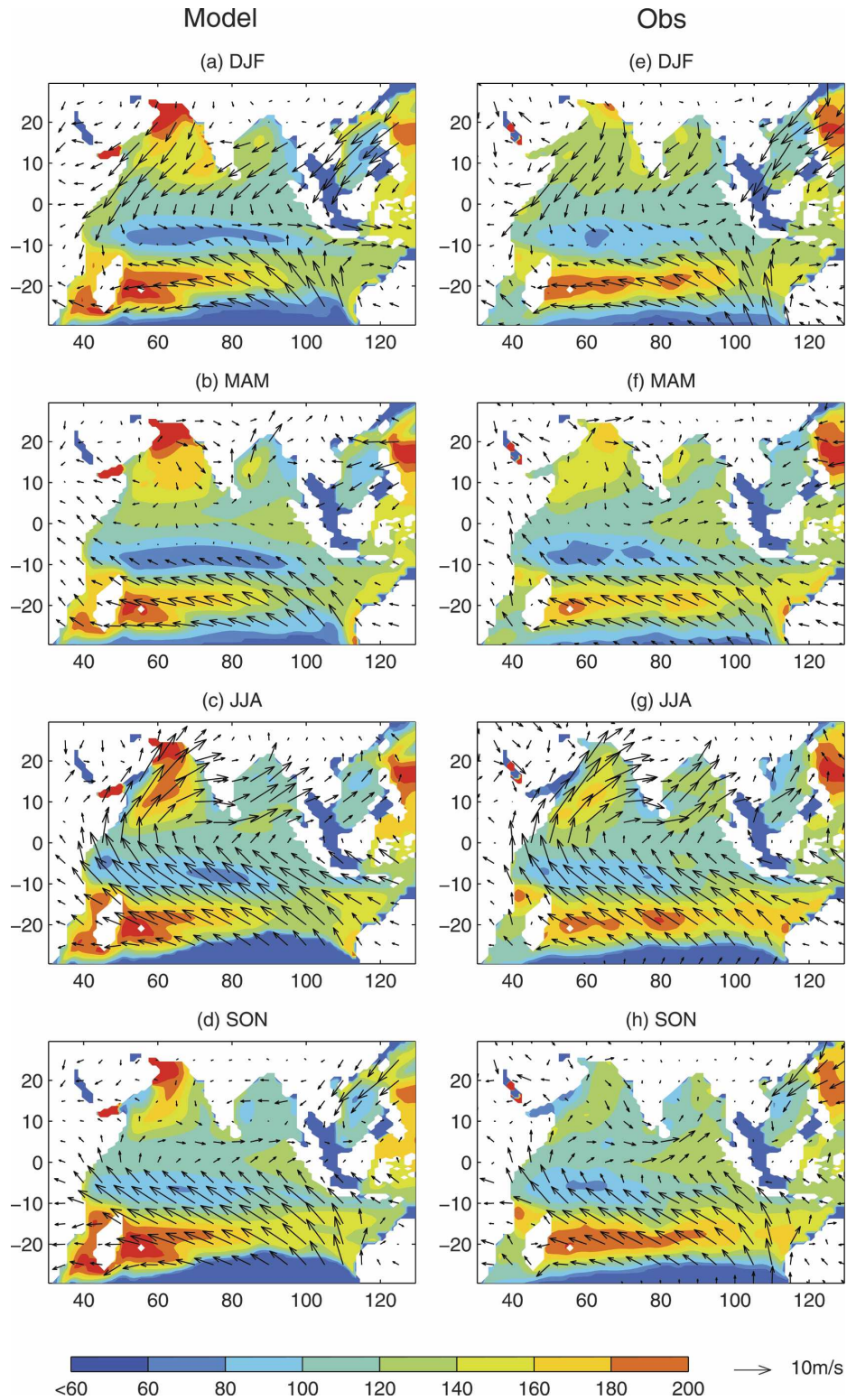


FIG. 1. Annual cycle of the depth of the 20°C isotherm (shaded) and surface winds (arrows) as (a)–(d) simulated in the model and (e)–(h) derived from Levitus temperature data and ECMWF wind product (averaged over 1986–2001).

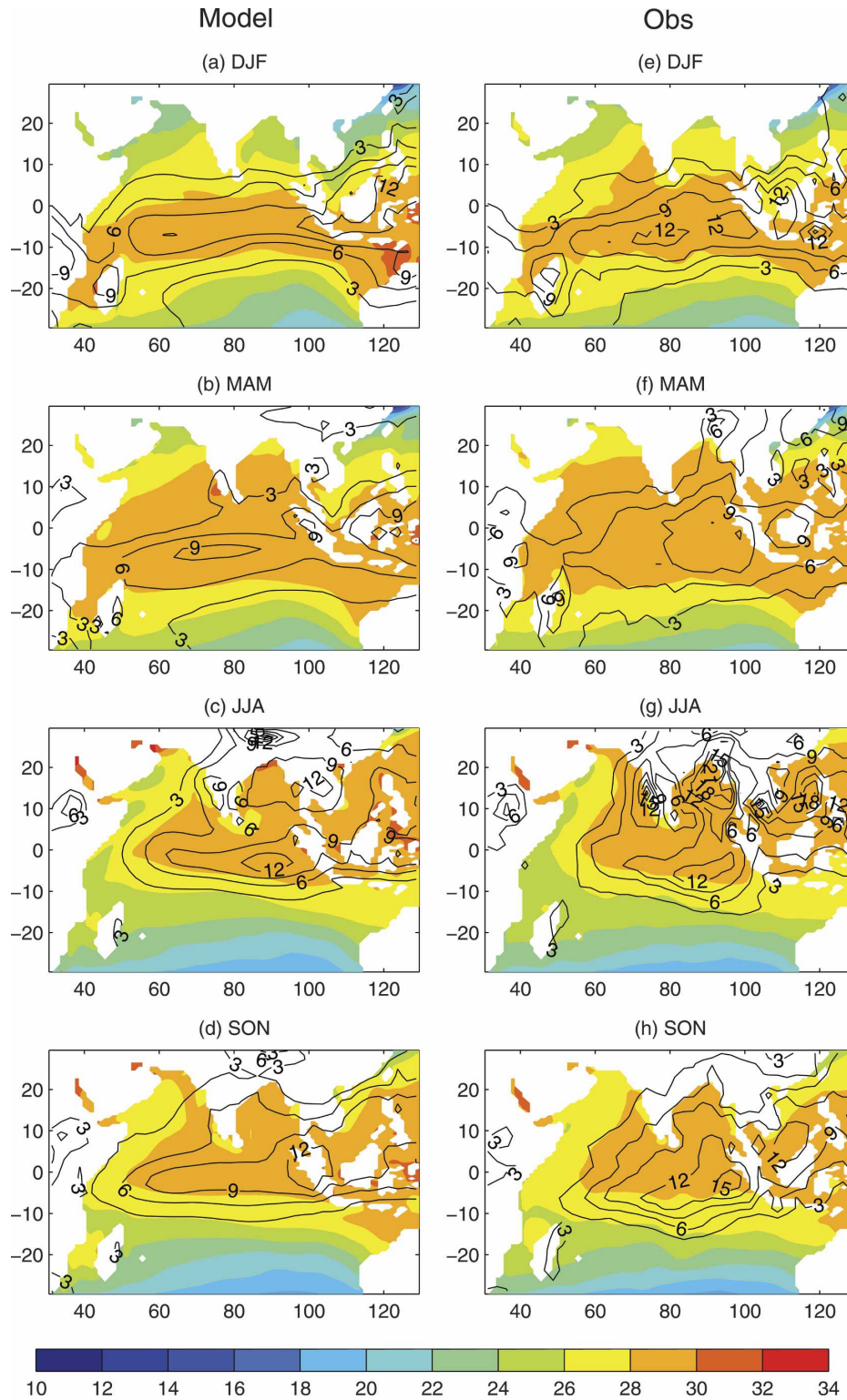


FIG. 2. As in Fig. 1 but for SST (shaded) and precipitation (mm day^{-1} , contours). Observations shown are from the Levitus temperature data and the Xie and Arkin (1996) precipitation data.

distinctive and robust feature of the observed Indian Ocean wind field.

b. Thermocline

We estimate the thermocline depth as the depth of the 20°C isotherm (Z20), a widely used proxy. The model reproduces the thermocline ridge in the southwestern tropical Indian Ocean between about 5°–10°S and the thermocline trough centered at about 20°S. Due to the stronger southeast trades in the model, the South Equatorial Current is stronger than that observed (Cutler and Swallow 1984; Richardson and McKee 1989), and the meridional thermocline slope between 5° and 20°S is larger than that in the Levitus climatology.

The seasonal evolution of the Indian Ocean equatorial thermocline is distinctive. During the monsoon transition seasons the equatorial westerly winds result in a pronounced east–west thermocline gradient. As the equatorial easterlies during the monsoon seasons are weaker than the equatorial westerlies during the monsoon transition season, the annual mean equatorial Indian Ocean thermocline in the model is tilted downward from the west to the east, which is a characteristic feature of the equatorial Indian Ocean.

c. SST

The GFDL coupled model successfully simulates many of the prominent features of the Indian Ocean SST, and their annual cycle (Fig. 2). However, the model SST has a cold bias in the northern Arabian Sea (during December–May) and in the southern Indian Ocean, partly due to the strong surface winds in the model. Consistent with the observations, the annual cycle of the northern Indian Ocean SST has a strong semiannual component with minima in February and July, whereas that of the southern Indian Ocean has a typical annual cycle similar to the subtropics of the other two basins.

d. Precipitation

The model precipitation is generally more equatorially confined than the rainfall climatology of Xie and Arkin (1996) (Fig. 2). Nonetheless, the model simulates many of the principal features of the seasonal migration of precipitation (which follows the warmest SST), in particular the monsoon rainfall over India and the Bay of Bengal in boreal summer.

e. Eastern tropical Indian Ocean

The ETIO (10°S–0°, 90°–110°E) deserves more careful examination, as it is the region where strong inter-

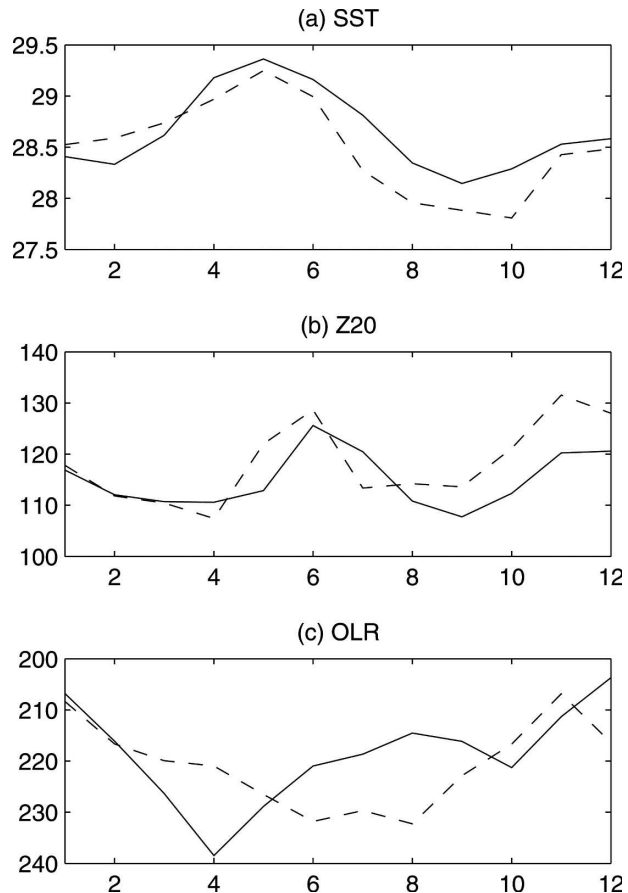


FIG. 3. Annual cycle of (a) SST, (b) Z20, and (c) OLR averaged over 10°S–0° and 90°–110°E, from the model (solid curves) and observations (dashed curves). Ocean temperature data are from the Levitus climatology, and OLR data are from the Climate Prediction Center (averaged over 1975–2004).

annual SST variability is observed (see section 4a) and it is important in the development of IODZM events. Consistent with the observations, the model SST in the ETIO has a prominent annual cycle with a maximum in May and a minimum in October (Fig. 3a), and the Z20 of the ETIO has a semiannual cycle with maximum in June and November (Fig. 3b) when the downwelling Kelvin pulses generated by the equatorial westerlies pass the Sumatra coast. The model OLR, however, has a phase shift relative to the observations (Fig. 3c). We also note that the model SST is warmer during most of the year, and the model thermocline is shallower during boreal fall and winter.

4. Interannual variability

a. Interannual sea surface temperature variability

The large-scale structure of the interannual SST variability in the CGCM is consistent with that in the ob-

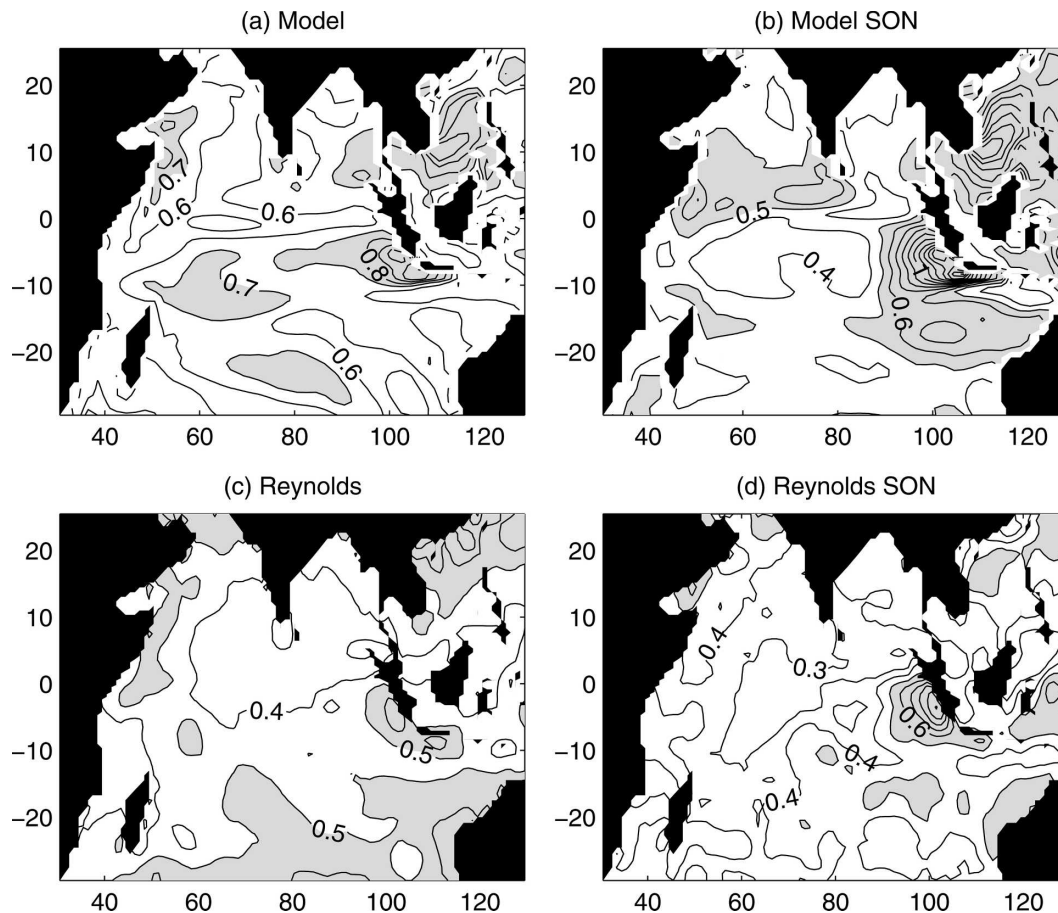


FIG. 4. Std dev of the monthly SSTA as computed from (a),(b) the model and (c),(d) the NOAA-OI SST dataset over the period 1982–2003. Both (a) and (c) are calculated from full-year time series, whereas (b) and (d) are calculated from boreal fall (SON)-only time series. Values greater than 0.7 in (a) and 0.5 in (b)–(d) are shaded.

servational record (Fig. 4). The modeled SSTA variation is the strongest in the upwelling regions along the coasts of Somalia and Java–Sumatra. Although the modeled interannual Indian Ocean SST variability is generally larger than that in observations (in particular off of Java–Sumatra), the model captures the observed seasonality of the interannual Indian Ocean SST variability. The modeled and observed ETIO SST variabilities peak during September–November (SON) (Figs. 4b and 4d).

We use empirical orthogonal function (EOF) decomposition to summarize the dominant patterns of the Indian Ocean SST variability (Fig. 5). The spatial patterns of the two leading EOFs from the model are similar to those from the observations. The first EOF (explaining 31% of the model SST variance) depicts the SST fluctuation of the same sign across the Indian basin. In the model, the simultaneous correlation between the first principal component and the Niño-3 index is 0.5 (sig-

nificant at 95% level), and the peak correlation is 0.72 (significant at 95% level) with Niño-3 leading the first principal component by 5 months. The magnitudes of these correlations agree with those from the observations. Krishnamurthy and Kirtman (2003) find a simultaneous correlation of 0.5 (over the time period of 1870–1998), and Yamagata et al. (2004) find a peak correlation of 0.8 when Niño-3 leads by 4 months (over 1958–99). These high lag correlations suggest that the first EOF represents a response of the Indian Ocean SST to ENSO, a suggestion that is consistent with composite analyses of El Niño (e.g., Harrison and Larkin 1998).

The second EOF (explaining 15.3% of the model SST variance) is the characteristic east–west dipole pattern that has been noted in many previous studies (e.g., Saji et al. 1999). The second principal component has a weaker correlation with Niño-3 than does the first principal component in the model, with a simultaneous cor-

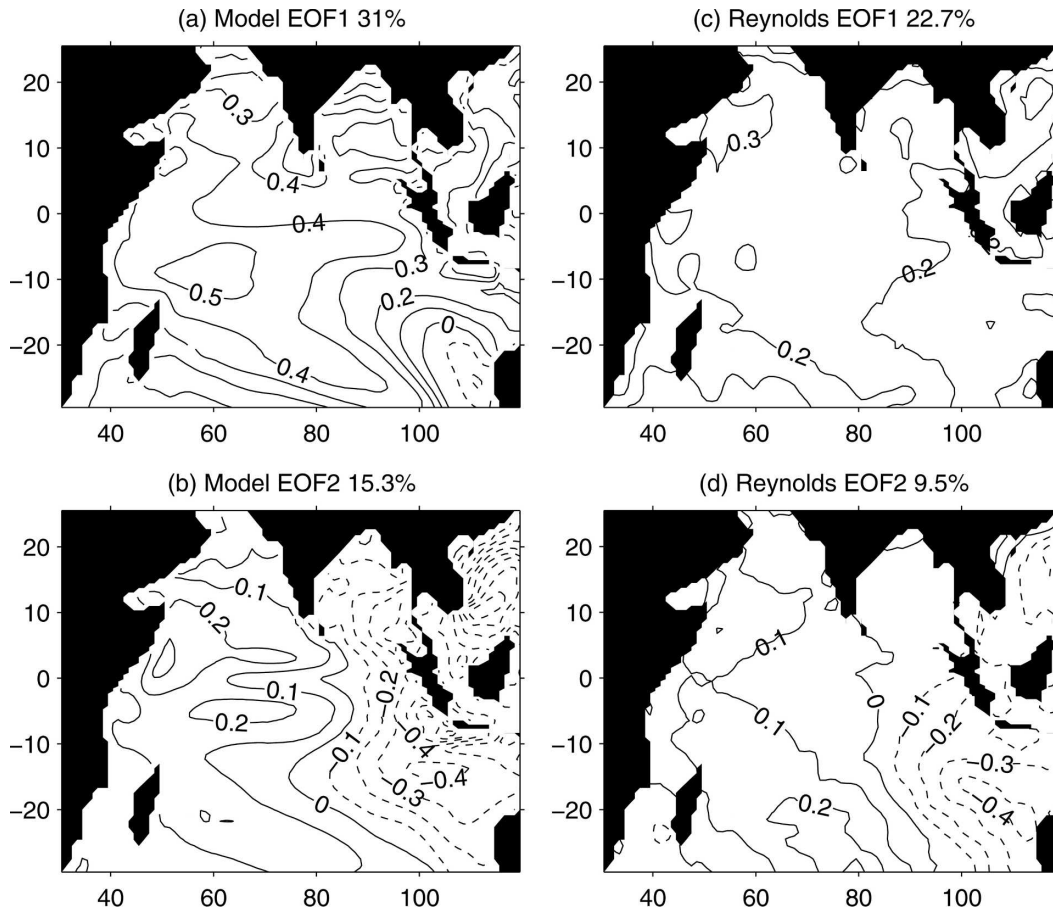


FIG. 5. The first two EOFs of the monthly SSTA as computed from (a),(b) the model and (c),(d) the NOAA-OI SST dataset over 1982–2003. The percentage of SST variance explained by each EOF is also shown.

relation of 0.36 (significant at the 95% level), and a peak correlation of 0.43 (significant at the 95% level) when Niño-3 lags the second principal component by 3 months. The striking east–west SST gradient of the second EOF prompted the definition of the Indian Ocean dipole index by Saji et al. (1999). The orthogonality of the EOF modes and the weak correlation between Niño-3 and the second principal component are among the factors noted in previous studies (e.g., Saji et al. 1999) to support the argument that the dipole mode is independent of ENSO. However, the interpretation of the statistical modes identified by EOF analysis as physical modes may be problematic (e.g., Dommenget and Latif 2002, 2003).

b. Indian Ocean dipole/zonal mode

In this study we adopt the IODZM index (referred to as IODZM-I hereafter) defined by Saji et al. (1999), which is the difference between the SSTA in the WTIO (10°S–10°N, 50°–70°E; referred to as WTIO-I hereaf-

ter) and the SSTA in the ETIO (10°S–0°, 90°–110°E; referred to as ETIO-I hereafter). The time series of the CGCM-simulated IODZM-I, Niño-3, WTIO-I, and ETIO-I are shown in Fig. 6, and their standard deviations are listed in Table 1, along with the same quantities obtained from the NOAA optimal interpolation (OI) SST (Reynolds et al. 2002) over the period 1982–2003. The interannual standard deviations of the indices are larger in the model than those in the NOAA-OI SST dataset, which is consistent with the stronger model SST variability (Fig. 4).

The model successfully reproduces many of the statistical characteristics of the IODZM and its relation with ENSO. The model IODZM-I exhibits prominent positive skewness. The skewness of the model IODZM-I is 0.91 (significant at the 95% level). The positive skewness of the IODZM-I is also found in other numerical model simulations (e.g., Gualdi et al. 2003) and observations—the skewness of the IODZM-I calculated from the NOAA extended SST dataset (Smith and

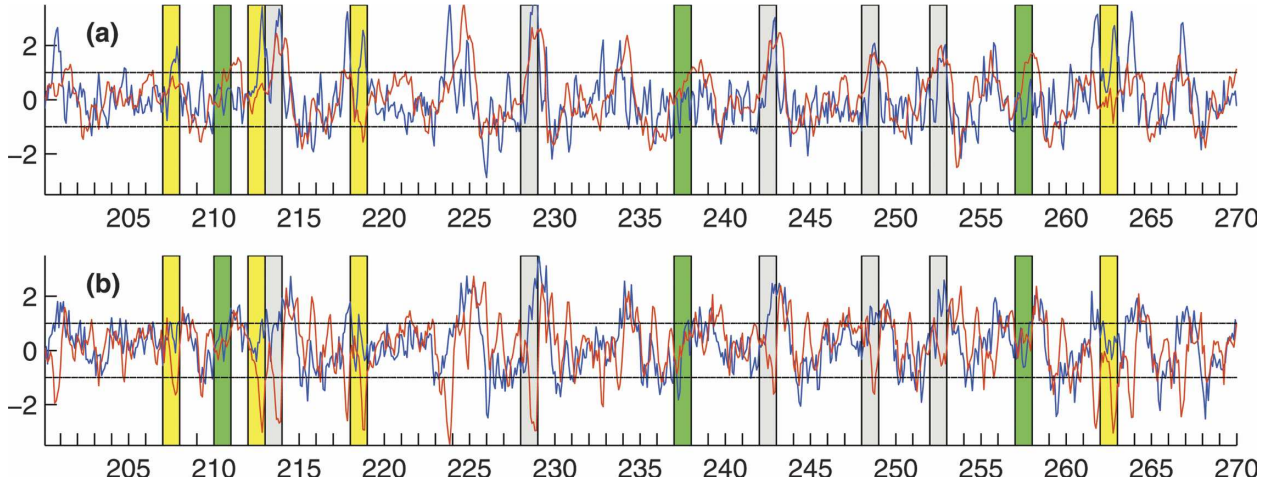


FIG. 6. Time series of (a) the IODZM index (blue) and the Niño-3 index (red), and (b) the WTIO index (blue) and the ETIO index (red). The indices are standardized. Values from years 201 to 270 are shown as an example. The superimposed bars indicate the years where only positive IODZM events (yellow), only El Niño events (green), or both positive IODZM and El Niño events (gray) occur.

Reynolds 2003) over 1950–2003 is 0.50 (significant at the 95% level).

As in the observations, the model positive extremes in the IODZM-I often co-occur with El Niño events, but not always. The correlation coefficients among various indices are shown in Table 2; the small difference between the correlations calculated from the model and from the observational data is likely due to the different lengths of the model and observational data, as the correlation coefficients have considerable interdecadal variation (see section 6b). The principal relationships between the indices shown in Table 2, evident in both model and observations, are

- 1) a relatively weak all-season correlation between Niño-3 and IODZM-I, but a significant positive correlation during the SON season;
- 2) a nominally negative, but not statistically significant, correlation between Niño-3 and ETIO-I, which becomes significantly negative during the SON season;
- 3) a strong, significant, and positive correlation between Niño-3 and WTIO-I, both through all seasons and during SON;
- 4) the negative correlation coefficient between WTIO-I and ETIO-I is robust and significant only during the SON season; and
- 5) a negative and significant correlation coefficient be-

TABLE 1. Std dev ($^{\circ}\text{C}$) of various time series

	IODZM-I	Niño-3	WTIO-I	ETIO-I
Model (250 yr)	0.72	1.35	0.50	0.63
NOAA-OI (1982–2003)	0.48	1.05	0.32	0.41

tween IODZM-I and the central equatorial Indian Ocean zonal wind anomaly (averaged over 5°S – 5°N , 70° – 90°E).

To focus on IODZM events of significant magnitude and their relationship to ENSO, we use the following criteria to define the IODZM and ENSO events:

- IODZM positive (negative) events:* IODZM-I $> 1\sigma$ ($< -1\sigma$) for five consecutive months
ENSO positive (negative) events: Niño-3 $> 1\sigma$ ($< -1\sigma$) for five consecutive months

The identified IODZM and ENSO events during the 250-yr model simulation are shown in Fig. 7. The positive skewness of the IODZM-I results in more positive than negative IODZM events. Saji and Yamagata (2003) use weaker criteria (an IODZM event is defined

TABLE 2. Cross-correlation coefficients for IODZM-I, WTIO-I, ETIO-I, Niño-3, and U_{eq} . Values *not* significant at the 95% level are set in italics. The U_{eq} data are adopted from the NCEP–NCAR reanalysis.

	Model (250 yr)		NOAA-OI (1982–2003)	
	Full year	SON only	Full year	SON only
ρ (Niño-3, IODZM-I)	0.30	0.53	0.38	0.75
ρ (Niño-3, ETIO-I)	<i>0.11</i>	<i>-0.39</i>	<i>-0.05</i>	<i>-0.64</i>
ρ (Niño-3, WTIO-I)	0.57	0.60	0.50	0.68
ρ (WTIO-I, ETIO-I)	0.19	<i>-0.50</i>	0.14	<i>-0.44</i>
ρ (U_{eq} , ETIO-I)	0.26	0.86	0.32	0.85
ρ (U_{eq} , IODZM-I)	<i>-0.60</i>	<i>-0.93</i>	<i>-0.58</i>	<i>-0.92</i>

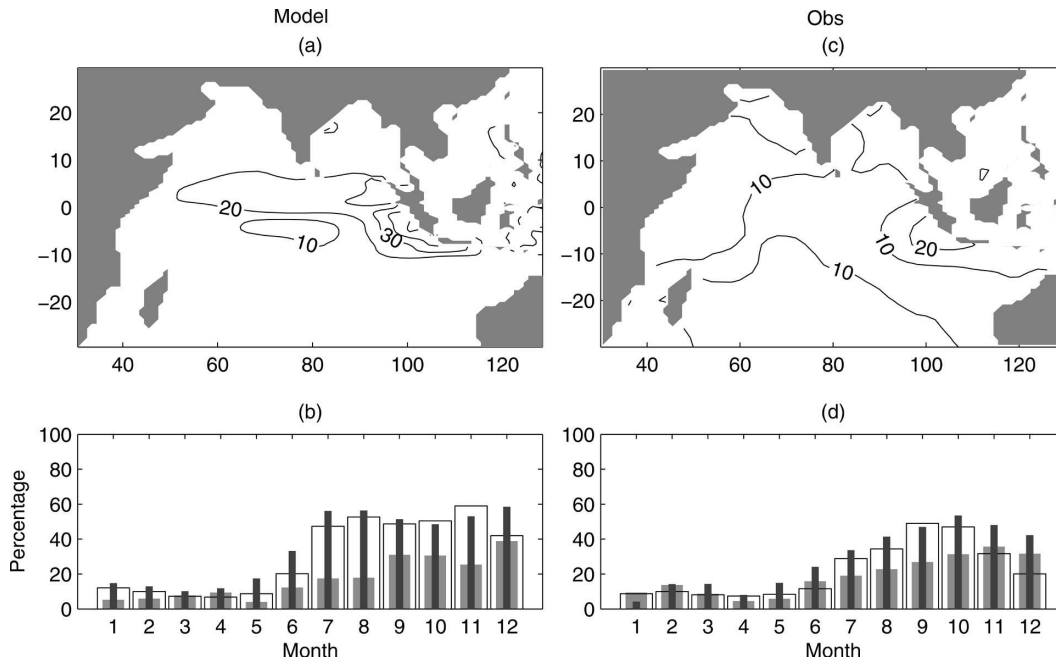


FIG. 8. (a) Percentage of total SST variance contributed by positive IODZM events at each of the locations in the Indian Ocean [see Eq. (1)]. (b) Percentage of the monthly variance of IODZM-I (thin black bars), ETIO-I (transparent bars), and WTIO-I (gray bars) contributed by positive IODZM events. (c),(d) Same as (a) and (b), respectively, but calculated from the NOAA extended SST dataset over the period 1950–2003.

tribution to the variability of WTIO-I is weak throughout the year. The aforementioned features are also evident in the observations (Figs. 8c and 8d).

5. Composite analysis

Composite analysis is used to further explore the air–sea coupled variability during the evolution of the IODZM, and the relationship between the IODZM and ENSO. We use the criteria described in section 4b to define IODZM and ENSO episodes, and the evolution of the following three groups of events is studied in this section.

IODZM-Only group (number of events = 8): positive IODZM episodes do not co-occur with positive ENSO episodes. We set a stringent criterion on the non-El Niño event condition to exclude weak El Niño events: that the Niño-3 index never exceeds 1σ during the period from January of the IODZM year until March of the following year.

ElNiño-Only group (number of events = 10): positive ENSO episodes do not co-occur with positive IODZM episodes. We exclude weak positive IODZM events by requiring that IODZM-I never exceed 1σ during the El Niño year (January–December).

IODZM+ElNiño group (number of events = 15): positive IODZM episodes and positive ENSO episodes coincide.

Examples of the selection criteria for events from each of the three groups are illustrated in Fig. 6. We now describe the composite evolution of each group.

a. IODZM-Only group

The composite anomaly fields of the SST, precipitation, surface winds, upper-ocean heat content, and SLP of this group are shown in Figs. 9a–h. The IODZM events simulated in the model exhibit strong seasonal phase-locking, consistent with that in other studies (e.g., Saji et al. 1999; Webster et al. 1999; Lau and Nath 2004; Gualdi et al. 2003).

In boreal spring (March–May; Figs. 9a and 9b), anomalous surface winds are southeasterly along Java–Sumatra and easterly along the equator, associated with the above-normal SLP over the southeastern tropical Indian Ocean. The wind anomalies act to shallow the thermocline off of Java–Sumatra and to deepen the thermocline to its southwest (5° – 10° S, 80° – 100° E), seen in the upper-ocean heat content field.

During boreal summer (June–August; Figs. 9c and 9d), the anomalous southeasterly winds along Java–Sumatra intensify. The upwelling induced by the along-

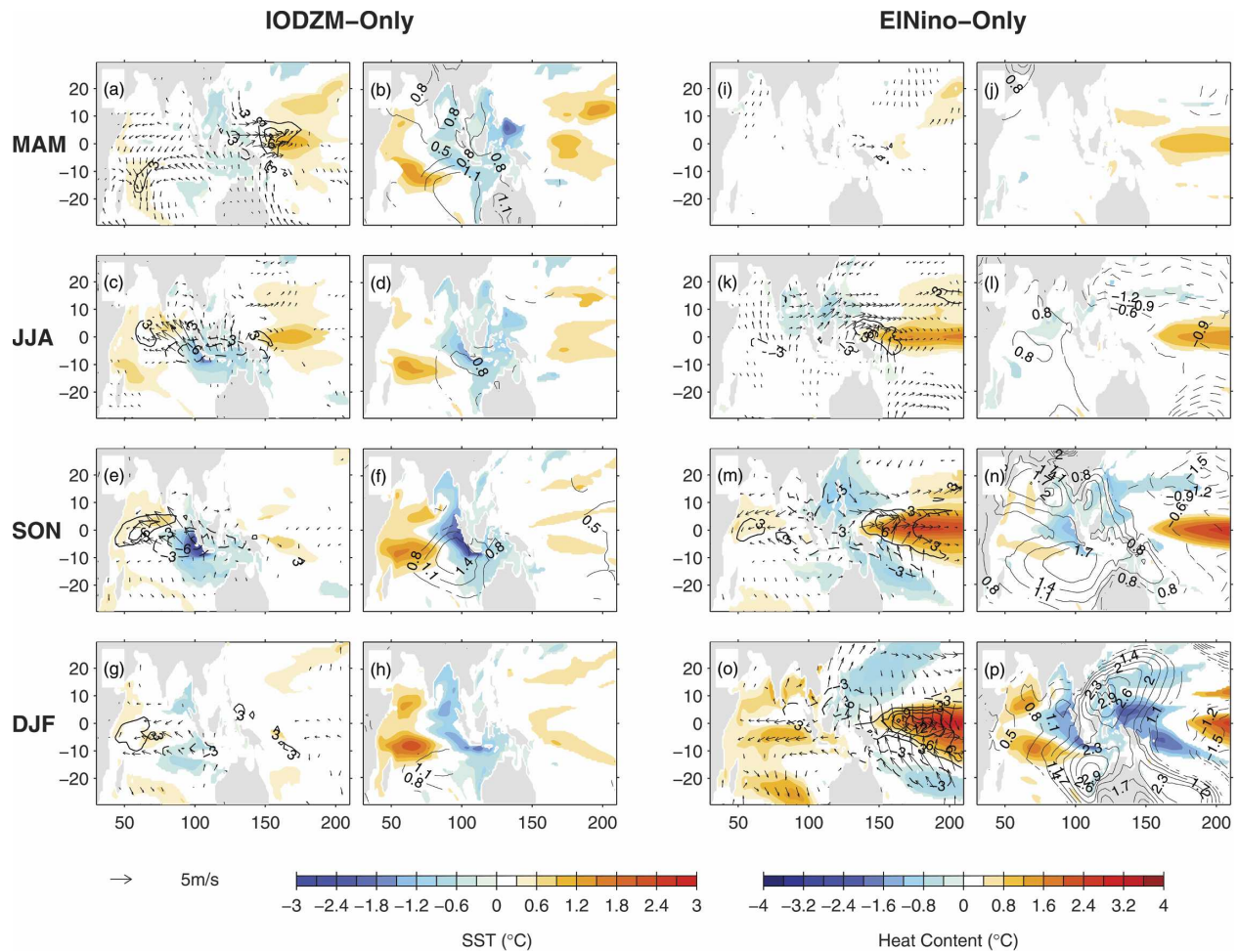


FIG. 9. Composite fields for the MAM, JJA, SON, and DJF seasons for the (left) IODZM-Only group and (right) ElNiño-Only group. The first and third columns are the composite fields of SST (shaded), precipitation (mm day^{-1} , contour; dashed curves represent negative values), and surface winds (arrows); the second and fourth columns are the composite fields of the upper-ocean heat content (shaded; calculated as the average temperature in the upper 200 m) and sea level pressure (contour; dashed curves represent negative values). Only values significant at the 95% level are shown. The contour interval for SLP is 0.3 hPa.

shore winds further raises the thermocline off of Java–Sumatra and causes surface cooling. Associated with the cool SSTa is below-normal precipitation over the ETIO. Meanwhile, the western Indian Ocean SSTa warms.

The composite model IODZM anomalies in the Indian Ocean reach their maximum by boreal fall (September–November; Figs. 9e and 9f): maximum ETIO surface cooling $\sim 3^{\circ}\text{C}$ and maximum WTIO surface warming of $\sim 0.8^{\circ}\text{C}$, comparable to the observed SSTa in boreal fall of the 1994 and 1997 IODZM events. The surface cooling in the eastern Indian Ocean is mostly due to anomalous entrainment. The surface warming in the western Indian Ocean can be principally attributed to anomalous horizontal temperature advection; anomalously westward surface currents are driven by

the equatorial easterly wind anomalies. Meanwhile, the anomalous net surface heat fluxes over the ETIO and WTIO act to damp, rather than amplify, the SSTa signal. The negative ETIO heat content anomaly remains; the positive WTIO heat content anomalies are principally off-equatorial, with larger magnitude south of the equator.

The precipitation anomalies also display a similar east–west asymmetric pattern. The above-normal WTIO precipitation is consistent with the anomalous low-level surface wind convergence. In the Gill (1980) framework, the below-normal ETIO precipitation would act to enhance the ETIO positive SLP anomaly south of the equator and the anticyclonic surface wind anomalies over much of the equatorial and southern Indian Ocean.

By boreal winter (December–February) the anomalous atmospheric fields in the Indian Ocean substantially weaken. The surface cooling in the ETIO virtually disappears, whereas there are still notable heat content anomalies with the characteristic dipole structure.

The characteristics of the composite IODZM events in this model agree with previous studies (e.g., Saji et al. 1999; Webster et al. 1999; Li et al. 2002, 2003; Annamalai et al. 2003; Gualdi et al. 2003; Yamagata et al. 2004; Lau and Nath 2004; Wajsovicz 2004). The evolution of the composite IODZM suggests that the growth of anomalous fields in the ETIO can be attributed to an atmosphere–ocean coupled feedback: positive SLP anomaly → anomalous southeasterly/easterly surface winds → stronger upwelling off of Java–Sumatra → cold SSTA → negative precipitation anomaly → positive SLP anomaly.

b. *El Niño-Only group*

The composite anomalies of this group (Figs. 9i–p) illustrate the El Niño forcing on the Indian Ocean in this CGCM.

The anomalies in the Indian Ocean induced by El Niño are noticeable beginning in the boreal fall of the developing stage of El Niño (Figs. 9m and 9n). A salient feature is the presence of two high SLP anomaly centers in the northern and southeastern Indian Ocean. These SLP features are consistent with the Rossby wave response to reduced diabatic heating caused by the eastward shift of deep convection (Lau and Nath 2003). Associated with the high SLP anomalies are anticyclonic atmospheric circulation features in each hemisphere (Fig. 9m). The anomalous southeasterly surface winds along Java–Sumatra act to elevate the thermocline there (Fig. 9n), in a similar fashion to the evolution of the ETIO during the developing phase of IODZM events in the IODZM-Only group. Meanwhile, a warm SSTA develops in the northwestern tropical Indian Ocean principally due to anomalous zonal advection.

In boreal winter, the El Niño–induced SLP anomalies have a tripolar pattern in the eastern Indian Ocean and western Pacific Ocean (Fig. 9p). The Indian Ocean SSTA evolves into a basin-wide warming structure (Fig. 9o), which continues into the following spring and summer (not shown).

c. *IODZM+El Niño group*

The difference between this group (Figs. 10a–h) and the IODZM-Only group, together with the El Niño-Only group, enables us both to isolate the El Niño in-

fluence on the IODZM and evaluate the linearity of its influence. Although the temporal evolution of the mixed IODZM+El Niño qualitatively resembles that in the IODZM-Only group from boreal spring to fall, there are significant quantitative discrepancies between them.

The SLP anomaly over the eastern Indian Ocean is substantially larger in the IODZM+El Niño group during boreal summer and fall (cf. Figs. 10d and 10f with Figs. 9d and 9f). As a result of the stronger zonal gradient of the SLP anomaly across the equatorial Indian Ocean, the easterly surface wind anomaly and near-surface ocean current anomaly (not shown) in the WTIO are also stronger in the IODZM+El Niño group (cf. Figs. 10c and 10e with Figs. 9c and 9e). The larger westward ocean current anomaly causes stronger anomalous ocean heat transport into the WTIO, which results in greater positive SSTA (with maximum of $\sim 1.5^{\circ}\text{C}$) in the WTIO in boreal fall in the IODZM+El Niño group (cf. Figs. 10e with Fig. 9e). The observational study of Drbohlav et al. (2007) confirms that IODZM-related warm SSTA in the WTIO is stronger in El Niño years than in non-El Niño years. Therefore, the IODZM events that co-occur with El Niño have a sharper east–west asymmetric SSTA pattern than those that do not co-occur with El Niño.

We saw in the El Niño-Only group that El Niño alone can drive anomalies in the Indian Ocean that have similar patterns to those related to IODZM events. By comparing Figs. 10a–h and Figs. 10i–p, it is evident that the anomalous fields in the IODZM+El Niño group are quite similar to those from a linear superposition of the IODZM-Only group and the El Niño-Only group. This suggests that, to a large degree, El Niño and the IODZM interact linearly in this model; this point will be further discussed in section 7c.

6. Decadal variability

a. *Decadal modulation of the Indian Ocean dipole/zonal mode*

There is an observed decadal variation to the occurrence of IODZM events. For example, there are more IODZM events in the 1960s and 1990s than in the 1970s and 1980s. The IODZM events in the model have similar decadal variability behavior (Fig. 7), with events clustered within certain decades (e.g., years 210–230 and 260–270). Interestingly, these decades are the periods when fewer than average El Niño events occur. Similarly, certain decades with more than average El Niño events (e.g., years 111–120 and 171–180) do not correspond to enhanced IODZM activity. Thus, in this

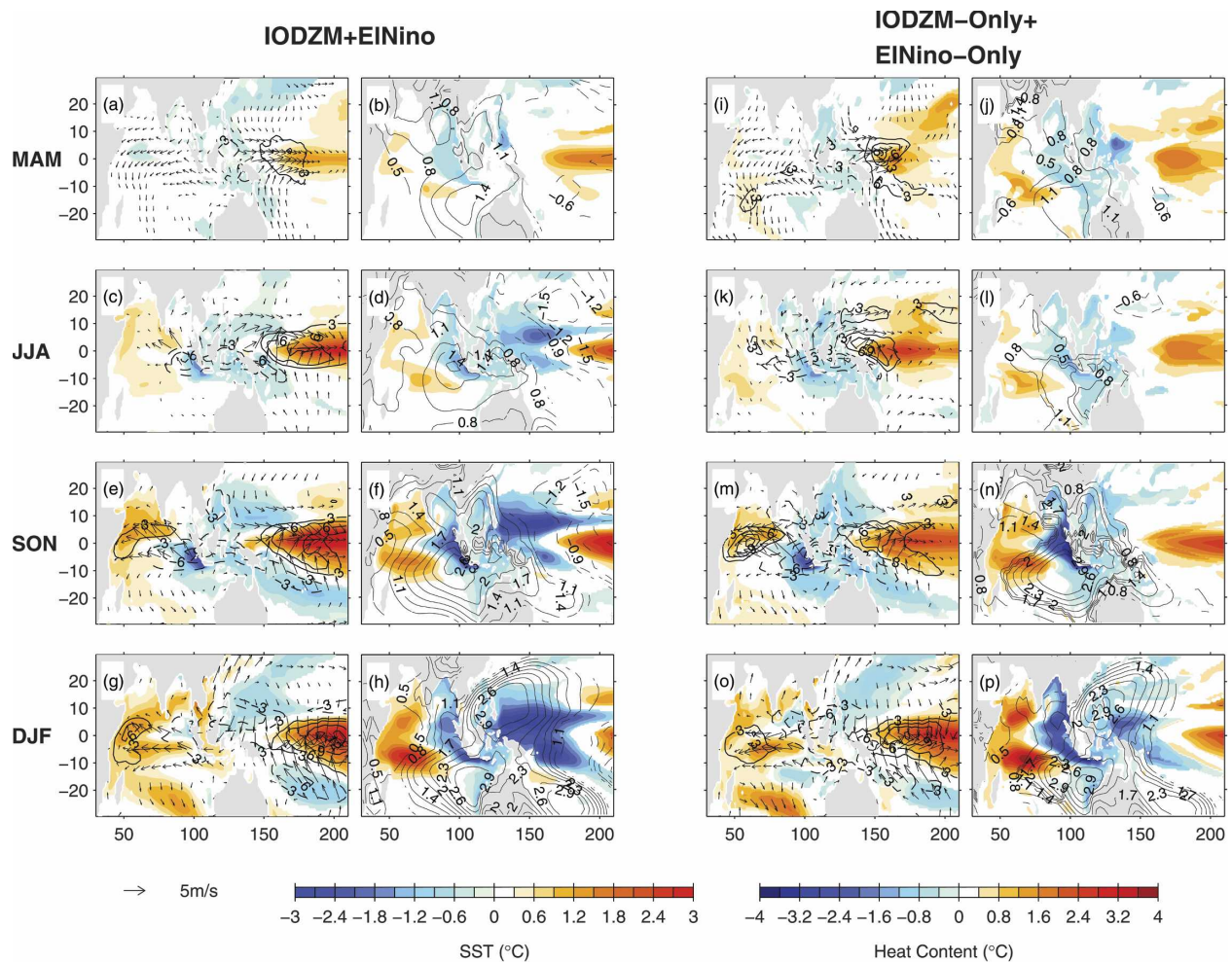


FIG. 10. Same as in Fig. 9 but for the composite fields of the IODZM+ElNiño group and the superimposition of the IODZM-Only group and the ElNiño-Only group.

model, the decadal modulation of the occurrence of IODZM events is not in phase with that of El Niño events. In fact, it appears to be somewhat out of phase: the time series of the number of IODZM events for each decade and that of the number of El Niño events for each decade are weakly anticorrelated (correlation coefficient = -0.36 , significant at the 90% level) during the 250-yr model simulation.

To explore the source of the decadal modulation of the occurrence of IODZM events, we look at the basic-state difference between the IODZM-active and IODZM-inactive decades. We choose the decades of years 151–160 (three events), 210–220 (four events), and 261–270 (four events) as the IODZM-active decades, and the decades of years 101–110 (zero events) and 231–240 (zero events) as the IODZM-inactive decades. The difference fields between the mean states of the IODZM-active and IODZM-inactive decades re-

semble the conditions of IODZM events (not shown), with cool SST in the ETIO, southeasterly winds along the coast of Java–Sumatra, and reduced precipitation over the ETIO. However, the difference patterns could be a result of the contribution of the IODZM years to the mean. To eliminate their contribution, we compute the basic state of the IODZM-active decades by only averaging the no-IODZM years in those decades. Then we find that the difference between the basic states of the IODZM-active and IODZM-inactive decades is not statistically significant (even at the 90% level), for both annual mean and seasonally stratified fields (not shown).

The lack of any significant difference between the basic states of the IODZM-active and IODZM-inactive decades suggests the possibility that the decadal variations may be an artifact of smoothing a series of randomly occurring IODZM events. We explore this hy-

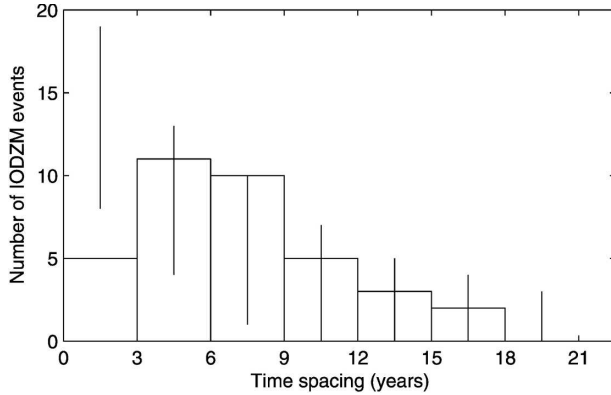


FIG. 11. Histogram of the time spacing between successive positive IODZM events. The lines are the 95% confidence intervals for the exponential distribution estimated using the Monte Carlo method.

pothesis by comparing the distribution of the time spacing between two successive IODZM events and an exponential distribution, which is that expected for the spacing between realizations of a Poisson-distributed random process. If there were no significant departures from an exponential distribution, the null hypothesis that the occurrence of IODZM events resulted from a “memory less” random process could not be rejected. We first estimate the exponential factor by computing the average time interval between the IODZM events. Then a Monte Carlo method is used to compute the confidence intervals for the estimated exponential distribution. Figure 11 shows the histogram for the time spacing between successive IODZM events, and the lines are the 95% confidence intervals for the estimated exponential distribution. We can see that the distribution of the time spacing peaks in the 3–6-yr range, and there is significant departure from the exponential distribution in the 0–3-yr bin. Therefore, the null hypothesis that the occurrence of IODZM events is a Poisson-distributed random phenomenon is rejected at the 95% significance level. And the occurrence of IODZM events has a preferred time scale of 3–6 yr.

Based on this 250-yr CGCM simulation, we are not able to identify the fundamental reasons for the decadal modulation of the occurrence of IODZM events. This question needs to be further explored in future studies. But the statistical analysis presented here suggests that there may be underlying mechanisms for the observed IODZM interevent separation and, thus, perhaps their decadal modulation.

b. Decadal variation of IODZM–ENSO relation

As both the IODZM and ENSO exhibit considerable decadal variation in both the model and the observa-

tions, the statistical relations between IODZM and ENSO may be affected. We examine the decadal variations of the IODZM–ENSO relation by calculating the sliding 21-yr correlation coefficients among IODZM-I, ETIO-I, WTIO-I, and the Niño-3 index (for both all-season data and SON-only data). The resultant time series of the correlation coefficients (Fig. 12) indeed display considerable decadal variations during the 250-yr model simulation. For instance, the correlation between IODZM-I and Niño-3 varies from 0.07 to 0.51 for all-season data, and that between ETIO-I and Niño-3 varies from -0.85 to -0.09 for SON-only data. The substantial decadal variability of the correlation coefficients indicates that the observed relationship between the IODZM and ENSO, which has been calculated from a relatively short record, may be prone to substantial uncertainties.

Despite substantial decadal variations in some relationships, certain aspects of the correlation coefficients are persistent. The all-season correlation between IODZM-I and Niño-3 is weaker than their SON-only correlation, and ETIO-I and Niño-3 are only significantly anticorrelated during SON, as are ETIO-I and WTIO-I. Furthermore, the correlation between WTIO-I and Niño-3 is similar for all-season data and SON-only data.

7. Discussion

a. How is the IODZM initiated?

Clarifying what initiates an IODZM event is crucial to our ability to understand, model, and forecast it. Comparing the IODZM-Only group and the IODZM+ElNiño group, it appears that similar anomalous conditions prevail in the early phase of the IODZM development (boreal spring) of both groups: anomalous easterlies in the equatorial Indian Ocean, and in the western equatorial Pacific an eastward shift of deep convection, anomalous westerlies, and warm SST anomalies (Figs. 9a and 9b and Figs. 10a and 10b). In contrast, these anomalous conditions do not exist in boreal spring in the ElNiño-Only group (Figs. 9i and 9j); rather, they appear one season later, in boreal summer (Figs. 9k and 9l).

We show in Figs. 13a–c the near-equatorial zonal surface wind anomalies in the three groups. For the events in both the IODZM-Only and IODZM+ElNiño groups, easterly surface wind anomalies exist in the Indian Ocean and westerly anomalies exist in the western equatorial Pacific from January through May–June, accompanied by eastward movement of deep convection (not shown), whereas they do not appear in the ElNiño-Only group until May.

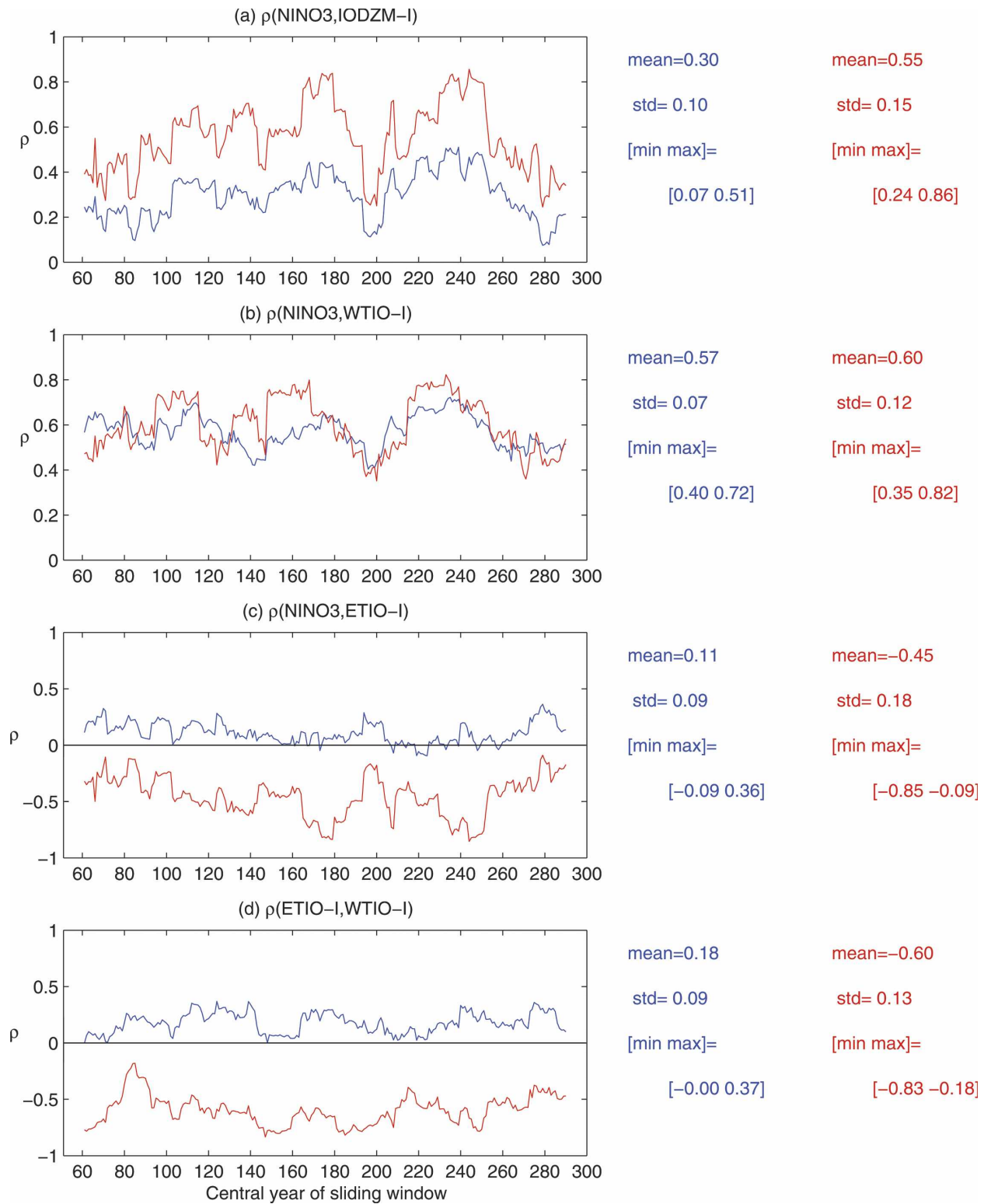


FIG. 12. The correlation coefficient between (a) Niño-3 and IODZM-I, (b) Niño-3 and WTIO-I, (c) Niño-3 and ETIO-I, and (d) ETIO-I and WTIO-I calculated within a sliding 21-yr window from model outputs of full-year data (blue) and SON-only data (red).

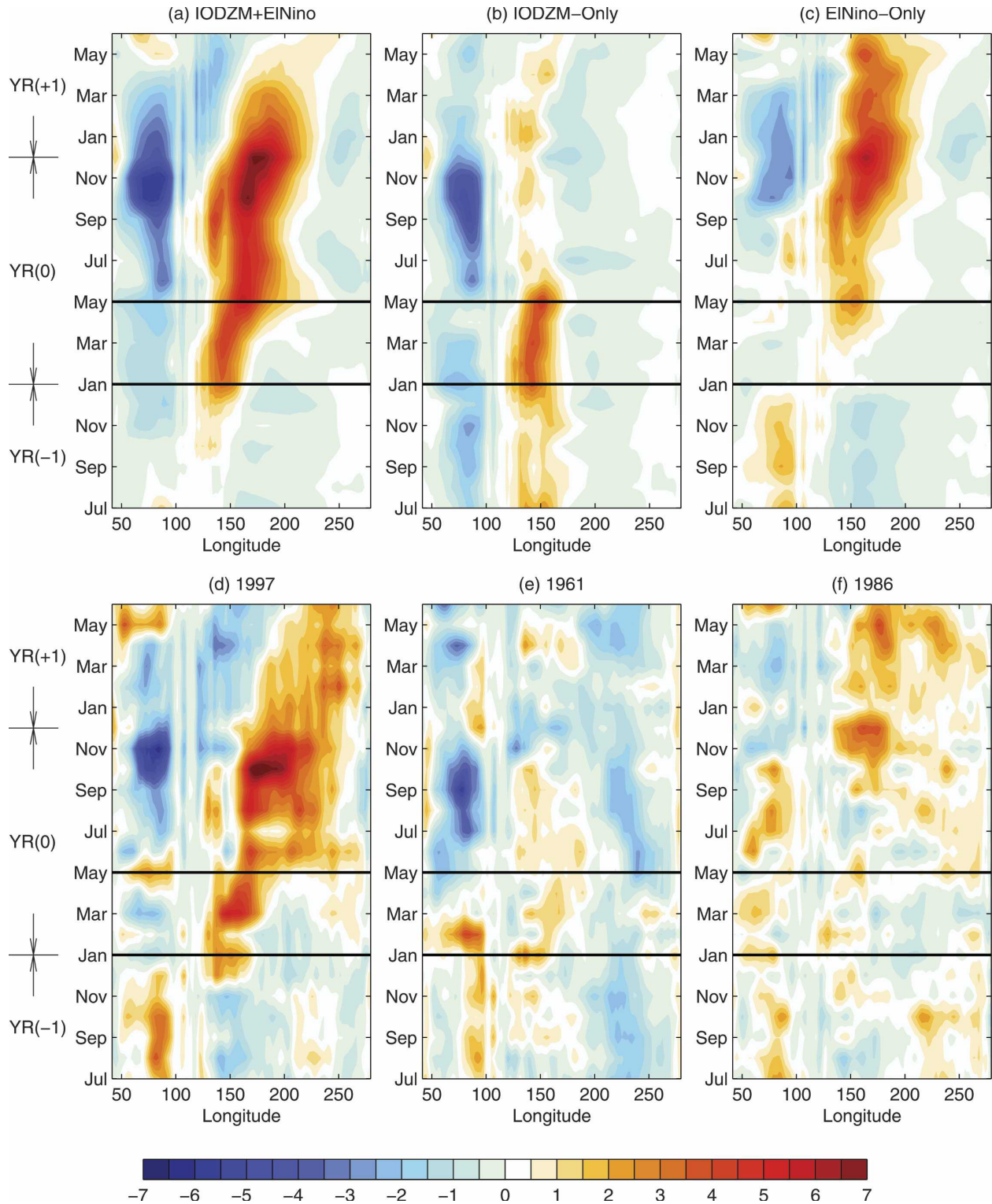


FIG. 13. Composite of the anomalous equatorial surface zonal wind (averaged between 5°S and 5°N) for (a) the IODZM+EINiño group, (b) the IODZM-Only group, (c) the EINiño-Only group from the model simulation, and (d) 1997, (e) 1961, and (f) 1986 from the NCEP-NCAR reanalysis.

An observational analog for the CGCM composite figures is shown in Figs. 13d–f. We shade the surface zonal wind anomalies obtained from the National Centers for Environmental Prediction–National Center for Atmospheric Research (NCEP–NCAR) reanalysis (Kalnay et al. 1996) in 1997, 1961, and 1986, which belong to the IODZM+ElNiño group, the IODZM-Only group, and the ElNiño-Only group, respectively. As in the model, there are anomalous equatorial westerlies in the western equatorial Pacific from January through May in both 1997 and 1961, but not in the boreal spring of 1986.

Therefore, we hypothesize that a boreal spring eastward shift of the warmest west Pacific SST and deep convection, and the associated divergence flow over the Maritime Continent, are important precursors of IODZM events. A possible explanation is that the eastward shift of deep convection produces anomalously negative diabatic heating of the atmosphere over the ETIO that induces an anticyclonic response in the SLP, thereby triggering the positive feedback over the ETIO (see section 5) that is essential for the growth of IODZM events. This hypothesis is supported by the observational analysis of Annamalai et al. (2003).

We are aware of two other hypothesized triggering mechanisms for IODZM events in the literature: SLP perturbation over the southeastern tropical Indian Ocean (Gualdi et al. 2003) and the Southern Annular Mode (SAM; see Lau and Nath 2004). As seen from Figs. 9b and 10b, a positive SLP anomaly in the southeastern tropical Indian Ocean appears during boreal spring for the IODZM events in both the IODZM+ElNiño and IODZM-Only groups. However, the SLP anomaly is not a feature independent of the anomalous conditions of the western equatorial Pacific. In fact, the correlation coefficient between the SLP perturbation in the southeastern tropical Indian Ocean and the SSTA in the western equatorial Pacific is 0.7. It could be that the development of the SLP anomaly in the southeastern Indian Ocean and the western Pacific convection shift represent two features of the same process.

The positive SLP anomaly south of Australia associated with the SAM in boreal summer (June–August), which Lau and Nath (2004) identify as a trigger for IODZM events when El Niño conditions do not prevail, is not a significant feature of our IODZM-Only composite (not shown). The reason for the discrepancy between this analysis and Lau and Nath (2004) is not clear to us, though different compositing criteria are a possibility. The connection among the SAM, the IODZM, and ENSO deserve attention in future studies.

b. Why do IODZM events not develop when favorable conditions exist?

Given the similarity in precursive conditions for the IODZM and El Niño, a question arises: why do IODZM events fail to develop when there exist favorable/precursive conditions, which are the eastward shift of deep convection and divergent surface winds over the Maritime Continent? In the context of this study, the question becomes why are there no IODZM events in the ElNiño-Only group? We suggest two reasons for this: 1) the timing of the appearance of precursive conditions and 2) the timing of the favorable conditions.

In the ElNiño-Only group there is a late appearance of the precursive conditions, in boreal summer rather than boreal spring (Figs. 13 a–c). Thus, a plausible explanation is that the IODZM events initiated in boreal spring are able to grow to a considerable size, but those initiated in summer may not be due to the short growth time. In fact, we find that in 5 of the 10 yr in the ElNiño-Only group the precursive conditions appear in summer. However, in the other 5 yr they appear in boreal spring.

So what are the inhibiting mechanisms during those 5 yr that have precursive patterns in springtime but with no IODZM development? Intraseasonal atmospheric variability in the ETIO during the early development of IODZM events (late boreal spring and early boreal summer) may play a role, as has been suggested by Gualdi et al. (2003). Tropical convective events normally form in the equatorial eastern Indian Ocean and propagate southwestward as they develop (e.g., Fig. 14). The surface winds associated with the convective events are westerly along the equator and northeasterly along the Java–Sumatra coast, both of which act to deepen the thermocline off of Java–Sumatra, acting to counter the IODZM growth from the thermocline–SST interaction.

In fact, there was a significant enhancement of intraseasonal convective variability in May–August in the 5 yr in which precursive conditions existed and the IODZM did not develop. In these 5 yr, the average number of May–August ETIO tropical convective events was four per year, which was larger than both the average number of convection events during the 250-yr model simulation (2.7) and the average number of convection events during the events in the combined IODZM+ElNiño group and the IODZM-Only group (1.5). As the CGCM was configured to output only monthly values of subsurface ocean variables, we are not able to quantify the impacts of tropical convection events on the IODZM evolution to substantiate our argument. However, observational (e.g., Harrison and

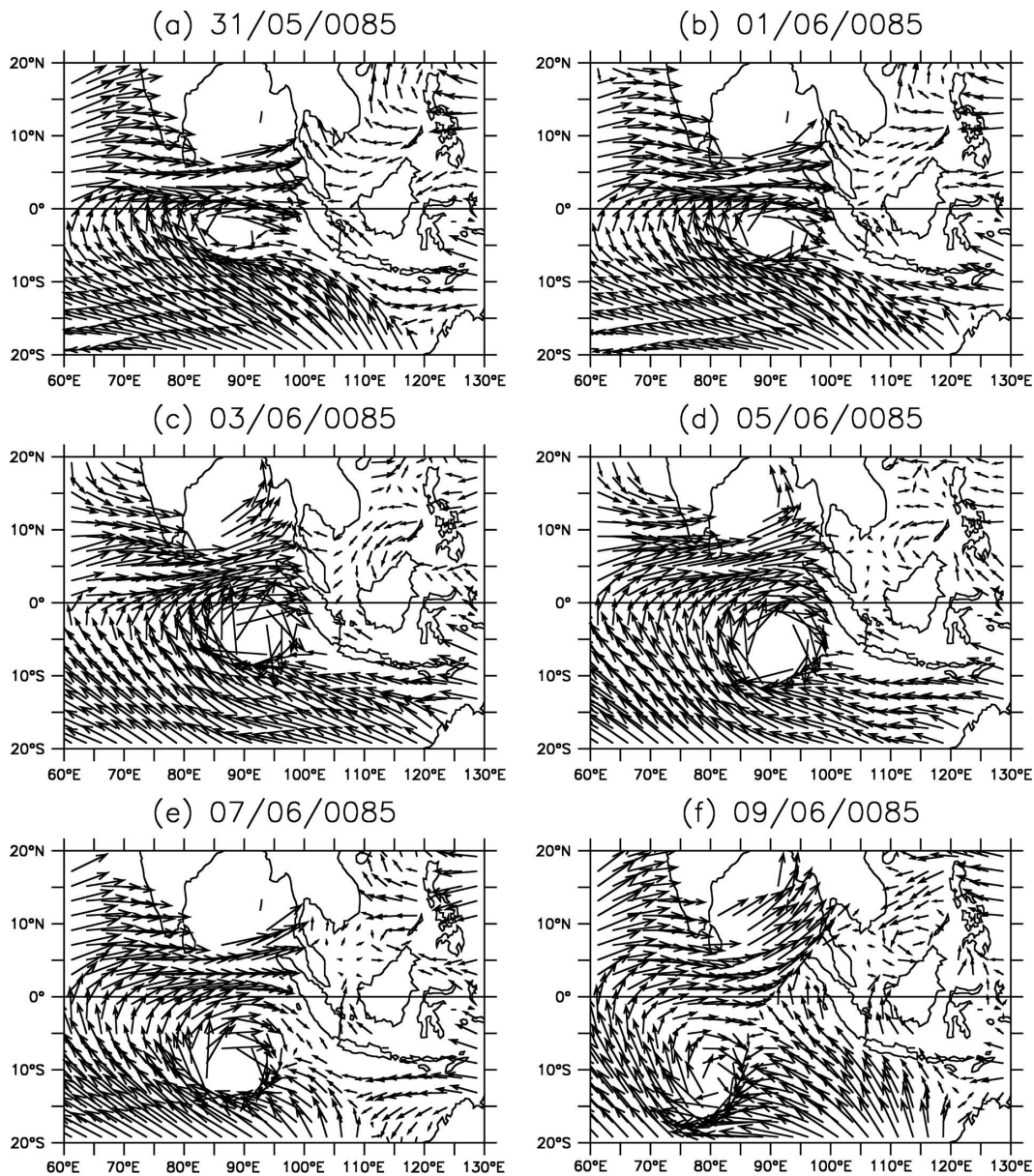


FIG. 14. Surface winds during a typical tropical convection event, which occurs from 31 May to 9 June in the model year 85, in the ETIO.

Vecchi 2001; Duvel et al. 2004; Masumoto et al. 2005) and modeling (e.g., Shinoda and Han 2005) studies have shown that intraseasonal convective variability is capable of generating a significant upper-ocean response in the eastern Indian Ocean.

c. Relation between the IODZM and ENSO

An interesting observation from the composite analysis is that the anomalous fields in the IODZM+ElNiño group are quite similar to those of the superposition of the IODZM-Only group and the ElNiño-Only group

(Fig. 10). In other words, the anomalies caused by El Niño and the IODZM in the Indian Ocean can be thought of as linearly independent of each other to some extent. That suggests El Niño- and IODZM-induced anomalies in the Indian Ocean have independent life cycles once the IODZM and El Niño events are initiated.

Some of the boreal springtime precursory signals for the IODZM that we identified in section 7a are also evident in boreal summer for the ElNiño-Only group. It has been observed that western and central Pacific

equatorial westerlies precede El Niño waveguide warming in the eastern equatorial Pacific (e.g., Wyrski 1975; Luther et al. 1983; Vecchi and Harrison 2000). It seems that there are common conditions that are favorable for the development of both IODZM and El Niño events. However, the anomalous patterns in the western equatorial Pacific are not uniquely associated with either the IODZM or El Niño, as they can appear without either an IODZM or El Niño event developing. We speculate that El Niño may not be the ultimate driving force for the IODZM. Rather, the IODZM and ENSO are two modes of a large-scale variability in the Indo-Pacific region, in which the tropical deep convection plays a central role, and the failure of one to develop does not appear to fundamentally impact the ability of the other to develop. In other words, though the favorable conditions are similar at the inception of IODZM and El Niño events, the development of each phenomenon does not require the other. This linear view appears to differ from previous conclusions that El Niño conditions favor the development of IODZM events (e.g., Annamalai et al. 2003), and that the IODZM may reinforce the development of El Niño conditions (e.g., Annamalai et al. 2005). The IODZM–ENSO relation remains to be clarified in future studies.

8. Conclusions

In this study we investigate the variability of the Indian Ocean in a 250-yr integration of the GFDL CM2.1 coupled atmosphere–ocean–land–ice model, with the focus placed on the IODZM and its relationship to ENSO. The coupled simulation reproduces many of the climatological features of the Indian Ocean climate system, as well as many aspects of the interannual variability.

The model reproduces the fundamental characteristics of the interannual SST variability of the Indian Ocean, the occurrence of IODZM events, and the statistical correlation between IODZM and ENSO. A composite analysis shows that local air–sea coupling is important for the development of IODZM-related anomalous fields in the eastern tropical Indian Ocean. As in the observational record, the model IODZM events may or may not co-occur with El Niño events. The model IODZM events that co-occur with El Niño have stronger anomalies and a sharper east–west SSTA contrast compared with those that occur without El Niño: El Niño can induce Indian Ocean anomalies that enhance some features of the IODZM; however, to a large extent, the El Niño impact on the IODZM in this CGCM appears to be linear.

In the model, there is considerable decadal modula-

tion to the occurrence of both IODZM and El Niño events. There is a weak negative correlation between the decadal occurrence of positive IODZM events and that of El Niño events. The statistics of the occurrence of IODZM events indicates that their decadal variation is not purely random, yet we have been unsuccessful in finding significant basic-state difference between the IODZM-active and IODZM-inactive decades. The mechanisms behind the decadal modulation of IODZM events need to be further studied. The statistical relationship between the IODZM and ENSO also exhibits substantial decadal variability. Hence, the statistical relationships between the IODZM and ENSO calculated from the relatively short observational record might be prone to uncertainties.

We suggest that the anomaly patterns over the Indo-Pacific warm pool (i.e., eastward shift of the warmest west Pacific SST and deep convection, and divergent surface winds over the Maritime Continent) are important precursors for the development of IODZM events. Furthermore, the timing of the onset of the precursive patterns is critical: those that appear in boreal spring are followed by IODZM events, but those that appear in boreal summer are often not. We speculate that the IODZM and El Niño are two separate large-scale phenomena of the Indo-Pacific system, which are connected by common favorable conditions for their initiation. However, after they are initiated, IODZM and El Niño can develop independently of each other, and each has its own coupled feedbacks that result in its characteristic life cycle.

In this study we have documented and evaluated the simulation of the climatological and interannual variabilities of the Indian Ocean in the GFDL CM2.1 CGCM. We have also proposed explanations, though somewhat speculative, for the key questions about the IODZM, such as its initiation and its relationship with ENSO. Further CGCM studies should be undertaken to clarify these issues.

Acknowledgments. This report was prepared by Dr. Qian Song under Award NA17RJ2612 from the National Oceanic and Atmospheric Administration, U.S. Department of Commerce. The authors are indebted to Dr. Joseph Sirutis for his kindness in providing us with the calculation of the number of tropical convection events in the Indian Ocean. GAV was supported by the Visiting Scientist Program at GFDL, administered by the University Corporation for Atmospheric Research (UCAR), and acknowledges helpful comments from Sebastian Ilcane. The paper benefited substantially from constructive comment and suggestions from Drs. Ngar-Cheung Lau, Jian Lu, and Andrew Wittenberg.

REFERENCES

- Allan, R. J., J. A. Lindesay, and C. J. C. Reason, 1995: Multidecadal variability in the climate system over the Indian Ocean region during the austral summer. *J. Climate*, **8**, 1853–1873.
- , and Coauthors, 2001: Is there an Indian Ocean dipole, and is it independent of the El Niño–Southern Oscillation? *CLIVAR Exchanges*, No. 21, International CLIVAR Project Office, Southampton, United Kingdom, 18–22. [Available online at <http://www.clivar.ucar.edu/publications/exchanges/ex21/spaper/s2106.pdf>.]
- Annamalai, H., and R. Murtugudde, 2004: Role of the Indian Ocean in regional climate variability. *Earth Climate: The Ocean–Atmosphere Interaction, Geophys. Monogr.*, Vol. 147, Amer. Geophys. Union, 213–246.
- , —, J. Potemra, S.-P. Xie, P. Liu, and B. Wang, 2003: Coupled dynamics over the Indian Ocean: Spring initiation of the zonal mode. *Deep-Sea Res. II*, **50**, 2305–2330.
- , S.-P. Xie, J. P. McCreary, and R. Murtugudde, 2005: Impact of Indian Ocean sea surface temperature on developing El Niño. *J. Climate*, **18**, 302–319.
- Baquero-Bernal, A., M. Latif, and S. Legutke, 2002: On the dipolelike variability of sea surface temperature in the tropical Indian Ocean. *J. Climate*, **15**, 1358–1368.
- Behera, S. K., S. P. Salvekar, and T. Yamagata, 1999: Unusual ocean–atmosphere conditions in the tropical Indian Ocean during 1994. *Geophys. Res. Lett.*, **26**, 3001–3004.
- , —, and —, 2000: Simulation of interannual SST variability in north Indian Ocean. *J. Climate*, **13**, 3487–3499.
- Bjerknes, J., 1969: Atmospheric teleconnections from the equatorial Pacific. *Mon. Wea. Rev.*, **97**, 163–172.
- CLIVAR–GOOS Indian Ocean Panel and Coauthors, 2006: Understanding the role of the Indian Ocean in the climate system—Implementation plan for sustained observations. WCRP Informal Rep. 5/2006, ICOP Publication Series 100, GOOS Rep. 152, 76 pp. [Available online at http://www.ioc-goos.org/index.php?option=com_oe&task=viewDoclistRecord&doclistID=3.]
- Cutler, A. N., and J. C. Swallow, 1984: Surface currents of the Indian Ocean (to 25°S, 100°E): Compiled from archived historical data. Met Office Rep. 187, Reading, United Kingdom, 42 pp.
- Delworth, T. L., and Coauthors, 2006: GFDL’s CM2 global coupled climate models. Part I: Formulation and simulation characteristics. *J. Climate*, **19**, 643–674.
- Dommenget, D., and M. Latif, 2002: A cautionary note on the interpretation of EOFs. *J. Climate*, **15**, 216–225.
- , and —, 2003: Reply. *J. Climate*, **16**, 1094–1097.
- Drbohlav, H.-K. L., S. Gualdi, and A. Navarra, 2007: A diagnostic study of the Indian Ocean dipole mode in El Niño and non-El Niño years. *J. Climate*, **20**, 2961–2977.
- Duvel, J., R. Roca, and J. Vialard, 2004: Ocean mixed layer temperature variations induced by intraseasonal convective perturbations over the Indian Ocean. *J. Atmos. Sci.*, **61**, 1004–1023.
- Gent, P., and J. McWilliams, 1990: Isopycnal mixing in ocean circulation models. *J. Phys. Oceanogr.*, **20**, 150–155.
- GFDL Global Atmospheric Model Development Team, 2004: The new GFDL global atmosphere and land model AM2–LM2: Evaluation with prescribed SST simulations. *J. Climate*, **17**, 4641–4673.
- Gill, A. E., 1980: Some simple solutions for heat-induced tropical circulation. *Quart. J. Roy. Meteor. Soc.*, **106**, 447–462.
- Gnanadesikan, A., and Coauthors, 2006: GFDL’s CM2 global coupled climate models. Part II: The baseline ocean simulation. *J. Climate*, **19**, 675–697.
- Griffies, S., 1998: The Gent–McWilliams skew flux. *J. Phys. Oceanogr.*, **28**, 831–841.
- , M. J. Harrison, R. C. Pacanowski, and A. Rosati, 2003: A technical guide to MOM4. GFDL Ocean Group Tech. Rep. 5, NOAA/Geophysical Fluid Dynamics Laboratory, Princeton, NJ, 295 pp.
- Gualdi, S., E. Guilyardi, A. Navarra, S. Masina, and P. Delecluse, 2003: The interannual variability in the Indian Ocean as simulated by a CGCM. *Climate Dyn.*, **20**, 567–582.
- Gutzler, D. S., and D. E. Harrison, 1987: The structure and evolution of seasonal wind anomalies over the near-equatorial eastern Indian Ocean and western Pacific Oceans. *Mon. Wea. Rev.*, **115**, 169–192.
- Harrison, D. E., and N. K. Larkin, 1998: El Niño–Southern Oscillation sea surface temperature and wind anomalies, 1946–1993. *Rev. Geophys.*, **36**, 353–399.
- , and G. A. Vecchi, 2001: January 1999 Indian Ocean cooling event. *Geophys. Res. Lett.*, **28**, 3717–3720.
- Hasternrath, S., 2002: Dipoles, temperature gradients, and tropical climate anomalies. *Bull. Amer. Meteor. Soc.*, **83**, 735–740.
- Huang, B., and J. L. Kinter III, 2002: Interannual variability in the tropical Indian Ocean. *J. Geophys. Res.*, **107**, 3199, doi:10.1029/2001JC001278.
- Iizuka, S., T. Matsuura, and T. Yamagata, 2000: The Indian Ocean SST dipole simulated in a coupled general circulation model. *Geophys. Res. Lett.*, **27**, 3369–3372.
- Kalnay, E., and Coauthors, 1996: The NCEP/NCAR 40-Year Reanalysis Project. *Bull. Amer. Meteor. Soc.*, **77**, 437–471.
- Klein, S. A., B. J. Soden, and N.-C. Lau, 1999: Remote sea surface temperature variations during ENSO: Evidence for a tropical atmospheric bridge. *J. Climate*, **12**, 917–932.
- Krishnamurthy, V., and B. P. Kirtman, 2003: Variability of the Indian Ocean: Relation to monsoon and ENSO. *Quart. J. Roy. Meteor. Soc.*, **129**, 1623–1646.
- Large, W. G., J. C. McWilliams, and S. C. Doney, 1994: Oceanic vertical mixing: A review and a model with a vertical K-profile boundary layer parameterization. *Rev. Geophys.*, **32**, 363–403.
- Lau, N.-C., and M. J. Nath, 2003: Atmosphere–ocean variations in the Indo-Pacific sector during ENSO episodes. *J. Climate*, **16**, 3–20.
- , and —, 2004: Coupled GCM simulation of atmosphere–ocean variability associated with zonally asymmetric SST changes in the tropical Indian Ocean. *J. Climate*, **17**, 245–265.
- Levitus, S., 1994: *World Ocean Atlas 1994: CD-ROM data set documentation*. NODC Informal Rep. 13, 30 pp.
- Li, T., Y. Zhang, E. Lu, and D. Wang, 2002: Relative role of dynamic and thermodynamic processes in the development of the Indian Ocean dipole: An OGCM diagnosis. *Geophys. Res. Lett.*, **29**, 2110, doi:10.1029/2002GL015789.
- , B. Wang, C.-P. Chang, and Y. Zhang, 2003: A theory for the Indian Ocean dipole–zonal mode. *J. Atmos. Sci.*, **60**, 2119–2135.
- Loschnigg, J., G. A. Meehl, P. J. Webster, J. M. Arblaster, and G. P. Compo, 2003: The Asian monsoon, the tropospheric biennial oscillation, and the Indian Ocean zonal mode in the NCAR CSM. *J. Climate*, **16**, 1617–1642.
- Luther, D. S., D. E. Harrison, and R. A. Knox, 1983: Zonal winds in the central equatorial Pacific and El Niño. *Science*, **222**, 327–330.

- Masumoto, Y., V. S. N. Murty, M. Jury, M. J. McPhaden, P. Hacker, J. Vialard, R. Molcard, and G. Meyers, 2003: Tropical Indian Ocean mooring array: Present status and future plans. *Proc. First Conf. of the Indian Ocean Global Ocean Observing System*, Grand Baie, Mauritius, UNESCO. [Available online at http://ioc.unesco.org/oopc/oopc9/Tropical_Indian_Moorings.pdf.]
- , H. Hase, Y. Kuroda, H. Matsuura, and K. Takeuchi, 2005: Intraseasonal variability in the upper layer currents observed in the eastern equatorial Indian Ocean. *Geophys. Res. Lett.*, **32**, L02607, doi:10.1029/2004GL021896.
- Meyers, G., and Coauthors, 2000: Monsoon, seasonal and interannual applications of an Indian Ocean observing system. *Observing the Ocean in the 21st Century*, C. J. Koblinsky and N. R. Smith, Eds., Bureau of Meteorology, 48–56.
- Murtugudde, R., and A. J. Busalacchi, 1999: Interannual variability of the dynamics and thermodynamics of the tropical Indian Ocean. *J. Climate*, **12**, 2300–2326.
- , J. P. McCreary, and A. J. Busalacchi, 2000: Oceanic processes associated with anomalous events in the Indian Ocean with relevance to 1997–1998. *J. Geophys. Res.*, **105**, 3295–3306.
- , A. J. Busalacchi, and J. P. McCreary, 2003: Comments on “Dipoles, temperature gradients, and tropical climate anomalies.” *Bull. Amer. Meteor. Soc.*, **84**, 1422–1423.
- Nigam, S., and H.-S. Shen, 1993: Structure of oceanic and atmospheric low-frequency variability over the tropical Pacific and Indian Ocean. Part I: COADS observations. *J. Climate*, **6**, 657–676.
- Rao, S. A., S. K. Behera, Y. Masumoto, and T. Yamagata, 2002: Interannual subsurface variability in the tropical Indian Ocean with a special emphasis on the Indian Ocean dipole. *Deep-Sea Res. II*, **49**, 1549–1572.
- Reynolds, R. W., N. A. Rayner, T. M. Smith, D. C. Stokes, and W. Wang, 2002: An improved in situ and satellite SST analysis for climate. *J. Climate*, **15**, 1609–1625.
- Richardson, P. L., and T. K. McKee, 1989: Surface velocity in the equatorial oceans (20°N–20°S) calculated from historical ship drifts. Woods Hole Oceanographic Institution Tech. Rep. WHOI-89-9, 50 pp.
- Saji, N. H., and T. Yamagata, 2003: Structure of SST and surface wind variability during Indian Ocean dipole mode events: COADS observations. *J. Climate*, **16**, 2735–2751.
- , B. N. Goswami, P. N. Vinayachandran, and T. Yamagata, 1999: A dipole mode in the tropical Indian Ocean. *Nature*, **401**, 360–363.
- Schott, A. F., and J. McCreary, 2001: The monsoon circulation of the Indian Ocean. *Prog. Oceanogr.*, **51**, 1–123.
- , M. Dengler, and R. Schoenefeldt, 2002: *Prog. Oceanogr.*, **51**, 57–103.
- Shinoda, T., and W. Han, 2005: Influence of Indian Ocean dipole on atmospheric subseasonal variability. *J. Climate*, **18**, 3891–3909.
- Smith, T. M., and R. W. Reynolds, 2003: Extended reconstruction of global sea surface temperatures based on COADS data (1845–1997). *J. Climate*, **16**, 1495–1510.
- Stouffer, R., and Coauthors, 2006: GFDL’s CM2 global coupled climate models. Part IV: Idealized climate response. *J. Climate*, **19**, 723–740.
- Tourre, Y. M., and W. B. White, 1995: ENSO signals in global upper ocean temperature. *J. Phys. Oceanogr.*, **25**, 1317–1332.
- Vecchi, G. A., and D. E. Harrison, 2000: Tropical Pacific sea surface temperature anomalies, El Niño, and equatorial westerly wind events. *J. Climate*, **13**, 1814–1830.
- , and —, 2004: Interannual Indian rainfall variability and Indian Ocean sea surface temperature anomalies. *Earth Climate: The Ocean–Atmosphere Interaction*, *Geophys. Monogr.*, Vol. 147, Amer. Geophys. Union, 247–260.
- Venzke, S., M. Latif, and A. Villwock, 2000: The coupled GCM ECHO-2. Part II: Indian Ocean response to ENSO. *J. Climate*, **13**, 1371–1383.
- Vinayachandran, P. N., S. Iizuka, and T. Yamagata, 2002: Indian Ocean dipole mode events in an ocean general circulation model. *Deep-Sea Res. II*, **49**, 1573–1596.
- Wajsovicz, R. C., 2004: Climate variability over the tropical Indian Ocean sector in the NSIPP seasonal forecast system. *J. Climate*, **17**, 4783–4804.
- Webster, P. J., A. M. Moore, J. P. Loschnigg, and R. R. Leben, 1999: Coupled ocean–atmosphere dynamics in the Indian Ocean during 1997–98. *Nature*, **401**, 356–360.
- Wittenberg, A. T., A. Rosati, N.-C. Lau, and J. J. Ploshay, 2006: GFDL’s CM2 global coupled climate models. Part III: Tropical Pacific climate and ENSO. *J. Climate*, **19**, 698–722.
- Wyrtki, K., 1973: An equatorial jet in the Indian Ocean. *Science*, **181**, 262–264.
- , 1975: El Niño—The dynamic response of the equatorial Pacific Ocean to atmospheric forcing. *J. Phys. Oceanogr.*, **5**, 572–584.
- Xie, P., and P. Arkin, 1996: Analysis of global monthly precipitation using gauge observations, satellite estimates, and numerical model predictions. *J. Climate*, **9**, 840–858.
- Xie, S.-P., H. Annamalai, F. A. Schott, and J. P. McCreary, 2002: Structure and mechanisms of South Indian Ocean climate variability. *J. Climate*, **15**, 864–878.
- Yamagata, T., S. K. Behera, J.-J. Luo, S. Masson, M. R. Jury, and S. A. Rao, 2004: Coupled ocean–atmosphere variability in the tropical Indian Ocean. *Earth Climate: The Ocean–Atmosphere Interaction*, *Geophys. Monogr.*, Vol. 147, Amer. Geophys. Union, 189–211.